How to Maneuver Around in Eccentricity Vector Space

Theodore H. Sweetser*
Jet Propulsion Laboratory, California Institute of Technology, Pasadena, California, 91109

The GRAIL mission to the Moon will be the first time that two separate robotic orbiters will be placed into formation in orbit around a body other than Earth. The need to design an efficient series of maneuvers to shape the orbits and phasing of the two orbiters after arrival presents a significant challenge to mission designers. This paper presents a simple geometric method for relating in-plane impulsive maneuvers to changes in the eccentricity vector, which determines the shape and orientation of an orbit in the orbit plane. Examples then show how such maneuvers can accommodate desired changes to other orbital elements such as period, incination, and longitude of the ascending node.

Nomenclature

a	=	semi-major axis
$\mathbf{a}_d$	=	a disturbing acceleration vector
C	=	a circle considered as a function of time
E	=	an ellipse considered as a function of time
e	=	eccentricity
e_x	=	the x component of $\mathbf{e}$
e_y	=	the y component of $\mathbf{e}$
$\mathbf{e}$	=	the eccentricity vector
M_0	=	the initial value of the mean anomaly
p	=	the semi-latus rectum
r	=	the magnitude of $\mathbf{r}$
$\mathbf{r}$	=	the position vector
R_P	=	the radial component of a perturbing acceleration
$\mathbf{s}$, $\mathbf{t}$, $\mathbf{u}$	=	position offset vectors
$\mathbf{s}'$, $\mathbf{t}'$, $\mathbf{u}'$	=	vectors which are vertical reflections of $\mathbf{s}$, $\mathbf{t}$, $\mathbf{u}$
T_P	=	the tangential component of a perturbing acceleration
v	=	the magnitude of $\mathbf{v}$
$\mathbf{v}$	=	the velocity vector
V	=	the magnitude of the velocity (used in Ref. 4)
α	=	the true anomaly at a point in an orbit (used in Ref. 4)
γ	=	flight path angle (from horizontal)
$\Delta\mathbf{v}$	=	the velocity change vector from an impulsive maneuver
$\Delta\mathbf{v}_R$	=	the radial component of $\Delta\mathbf{v}$
$\Delta\mathbf{v}_T$	=	the transverse component of $\Delta\mathbf{v}$
θ	=	the true anomaly at a point in an orbit
μ	=	the Gm of the central body
φ	=	an initial phase angle
ω	=	the argument of periapse
$\perp_\ell$	=	an operator which rotates a vector by -90 deg (i.e., a left-handed rotation)

* Mission Design Engineer, Guidance, Navigation, and Control Section, Mail Stop 301-121, AIAA Senior Member.

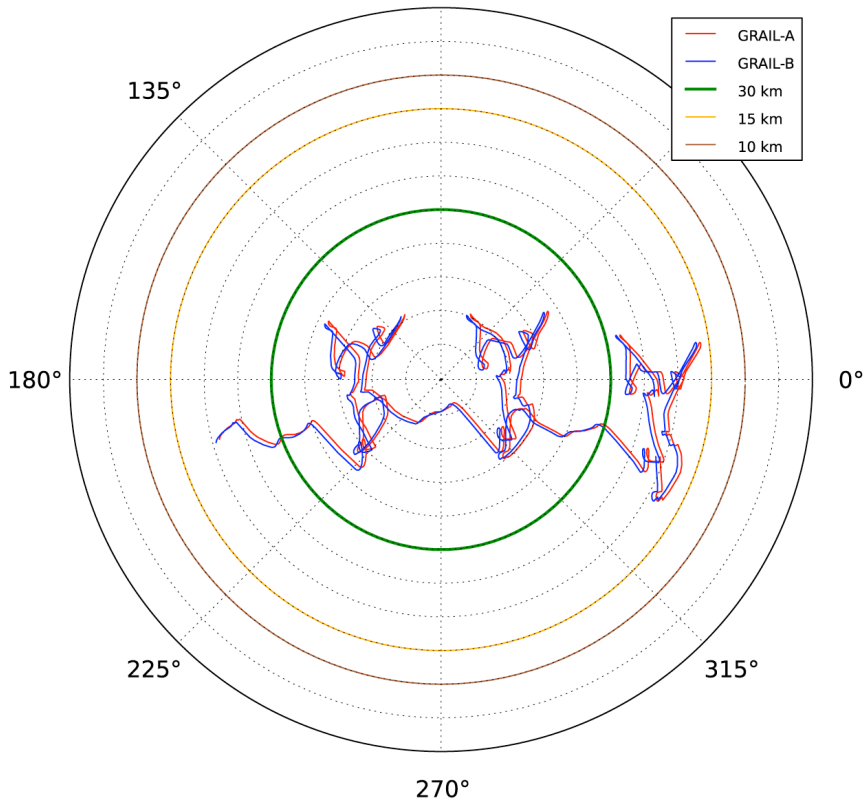

Figure 1. The eccentricity vector evolution for the orbits of GRAIL-A and GRAIL-B during the Science Phase of the GRAIL mission. The units used for eccentricity are periapse altitude in kilometers for an orbit with 55 km mean altitude. (Figure provided by Sara Hatch at JPL.)

I. Introduction

THE GRAIL mission[1] will launch two orbiters in the fall of 2011 to go to the Moon, where they will arrive a day apart on December 31, 2011, and January 1, 2012, and insert themselves into coplanar polar lunar orbits. A series of maneuvers will then be performed by each orbiter to circularize the orbits and in the process adjust the relative phasing of the orbiters so that they end up in the same low lunar orbit with an along-track separation of about 75 km. During these maneuvers, out-of-plane components will be included to correct orbit plane errors. The entire maneuver design for making this transition from the arrival orbits to the science orbit will be described in another paper[2]; this paper describes a method for understanding geometrically how to control changes in eccentricity e and argument of periapse ω, which make up a crucial part of that strategy, and how those changes can interact with desired changes in period and orbit plane.

The natural way to examine changes in e and ω is to combine them into an eccentricity vector $\mathbf{e}$, which has length e and angle ω in polar coordinates, so that if we identify the eccentricity vector space with the orbit plane the eccentricity vector points toward the periapse and when scaled by a, the semi-major axis, it is exactly the vector from the center of the orbit to the focus at which the central body sits. In Cartesian coordinates, $\mathbf{e} = (e\cos\omega, e\sin\omega)$, where the x-axis is the line of nodes, with the ascending node on the positive x-axis so that motion in the orbit is in the usual direction, i.e., the angle to the orbiter increases with time in this right-handed coordinate system.

The eccentricity vector space is particularly useful for seeing the evolution of an orbit under the influence of perturbations; Figure 1 shows how the GRAIL orbit shape and orientation at the Moon change during the three-month Science Phase. Note how easy it is to see that three months is as long as an orbiter can stay in low lunar orbit without doing a maneuver to change its eccentricity vector, and that in order to avoid orbit maintenance maneuvers for that long the eccentricity vector at the beginning of science needs to point close to the left edge of the plotted region (which is bounded by the eccentricity limit outside of which the periapse is below the lunar surface for this

size orbit). To make it easy to relate the orbit to the lunar surface, eccentricity is affinely transformed to the periapse index altitude (i.e., altitude with respect to a sphere whose radius is the mean equatorial radius of the Moon) for an orbit with a semi-major axis of 1792.4 km; thus the units for eccentricity in Figure 1 are kilometers and the origin is at 55 km.

The challenge that GRAIL presents to the mission designer is that the two orbiters arrive into large elliptical lunar orbits on 2011-12-31 and 2012-01-01 and must maneuver themselves into science formation and check out their instruments in time to begin science operations on 2012-03-08. The science formation has the two orbiters in the same orbit with a semi-major axis of 1792.6 km, with GRAIL-B about 85 km ahead of GRAIL-A at the start of the Science Phase, and with the separation slowly increasing at a rate of 4 km/day. The series of maneuvers[2] to do this must not only reduce the orbiter periods in such a way that the two orbiters end up with the right period and the right relative anomalies, but must also put the orbiters in the same orbit plane and with the same eccentricity vector at the left edge of the safe region in the eccentricity vector space shown in Figure 1. In the process the final maneuvers must compensate for the natural tendency of the eccentricity vector to move across to the right while all of this is being done. And of course we want to do this with the proper balance between the minimum number of maneuvers and the minimum total Δv.

II. Maneuvering to Change the Eccentricity Vector

There are two ways to look at the problem addressed here: given a desired change $\Delta\mathbf{e}$ in the eccentricity vector, what maneuver will accomplish it; conversely, given a maneuver, what effect will it have on the eccentricity vector $\mathbf{e}$? Actually the answer has been known for a long time, at least at the infinitesimal limit, and is derived vectorially[3]:

$$\mu\frac{d\mathbf{e}}{dt} = 2(\mathbf{v}\cdot\mathbf{a}_d)\mathbf{r} - (\mathbf{r}\cdot\mathbf{a}_d)\mathbf{v} - (\mathbf{r}\cdot\mathbf{v})\mathbf{a}_d\,. \qquad \text{(Eq. 10-75 in Ref. 3)}$$

When the orbit is circular so that $\mathbf{r}\cdot\mathbf{v}=0$, this can be reduced to a simpler form as follows, although these equations were derived in the reference[4] directly from Gauss's equations:

$$\begin{aligned}\frac{de_x}{dt} &= \frac{2\cos\alpha}{V}T_P + \frac{\sin\alpha}{V}R_P\,,\\ \frac{de_y}{dt} &= \frac{2\sin\alpha}{V}T_P - \frac{\cos\alpha}{V}R_P\,.\end{aligned} \qquad \text{(Eqn. in Ref. 4)}$$

We can see directly from these latter equations that when the perturbing acceleration is tangential, the change in the eccentricity vector is in the direction of the radius vector at the point at which the acceleration is applied; thus the direction of the eccentricity change is -90 deg from the direction of the acceleration, and this is true whether the acceleration is in the velocity direction or is opposite to it. Similarly, when the perturbing acceleration is radial, the direction of the eccentricity change is -90 deg from the direction of the acceleration. By the linearity of derivatives, we can take any maneuver and break it up into tangential and radial components; the change resulting in $\mathbf{e}$ from each component is -90 deg from that component's direction so that the total change would be -90 deg from the original maneuver except that the magnitude of the change from the tangential component is twice as big as the change from the radial component. It easy to show that the maximum deviation from the rough rule that "the change in $\mathbf{e}$ is at right angles clockwise from the maneuver direction" occurs when the maneuver direction is about 35 deg away from radial (more precisely, the arccosine of the square root of 2/3), and that in this case the direction of $\Delta\mathbf{e}$ is about -70.5 deg or -109.5 deg from the maneuver direction (more precisely, arccos(1/3)), depending on the signs of the components.

In the following sections I will use geometric methods to show that the above rule also applies to impulsive maneuvers on elliptical orbits to first order in e, i.e., ignoring terms in e^2 or higher, with a bit of a twist in the elliptical case. More explicitly, to first order in e, we have

$$\Delta\mathbf{e} \approx \frac{1}{v}\left(2\Delta\mathbf{v}_T + \Delta\mathbf{v}_R\right)^{\perp_\ell} \qquad (1)$$

where the symbol $\perp_\ell$ stands for the operation of rotating the vector perpendicularly to the left, i.e., by -90 deg, and where the meanings of transverse and radial in separating the maneuver into the components $\Delta\mathbf{v}_T$ and $\Delta\mathbf{v}_R$ have a bit of twist, which will be defined at the end of this section.

A. Easy Moves in Eccentricity Space I: Radial Maneuvers

A single impulse can be used to rotate the line of apsides (the major axis) of an orbit of eccentricity e and semi-major axis a through an angle $\Delta\omega$ in the plane of the orbit[5], where the size and shape of the orbit remain constant, since the initial and final orbits intersect. Specifically we can apply an impulse of magnitude

$$\|\Delta\mathbf{v}\| = 2e\sin\left(\frac{\Delta\omega}{2}\right)\sqrt{\frac{\mu}{a(1-e^2)}} \tag{2}$$

either at the intersection of the orbits near apoapse or at the intersection near periapse.

In order to derive this equation, let us first note that

$$\|\Delta\mathbf{v}\| = 2\dot{r} \quad \text{and} \quad \frac{\Delta\omega}{2} = \theta,$$

where r is the radius from the center of the gravitating body and θ is the true anomaly where the maneuver is done, at the intersection between the initial and rotated orbits. So we need to solve for $\dot{r}$ in terms of a, e, and θ for a given μ.

To start with we have Kepler's first law, conservation of energy, and conservation of angular momentum:

$$r = \frac{p}{1+e\cos\theta} \tag{3}$$

where p, the semi-latus rectum, equals $a(1-e^2)$;

$$\frac{-\mu}{2a} = \frac{v^2}{2} - \frac{\mu}{r} \tag{4}$$

where v is the magnitude of the velocity; and

$$r^2\dot{\theta} = rv\cos\gamma = \sqrt{\mu p} \tag{5}$$

where γ is the flight path angle (the last equality in Eq. (5) can be derived at periapse using the vis-viva equation, which is Eq. (4), and using the fact that the radius at periapse equals $a(1-e)$).

Equation (2) can then be derived by differentiating Eq. (3) with respect to time and plugging in Eq. (5):

$$\begin{aligned}\dot{r} &= \frac{p}{(1+e\cos\theta)^2}(-(-e\sin\theta)\dot{\theta}) \\ &= \frac{r^2}{p}e\sin\theta\frac{\sqrt{\mu p}}{r^2} \\ &= e\sin\theta\sqrt{\frac{\mu}{a(1-e^2)}}\end{aligned}$$

Figure 2 shows how such a radial maneuver changes the eccentricity vector. Note that from Eq. (2), if we ignore terms in e^2, then the magnitude of the change is:

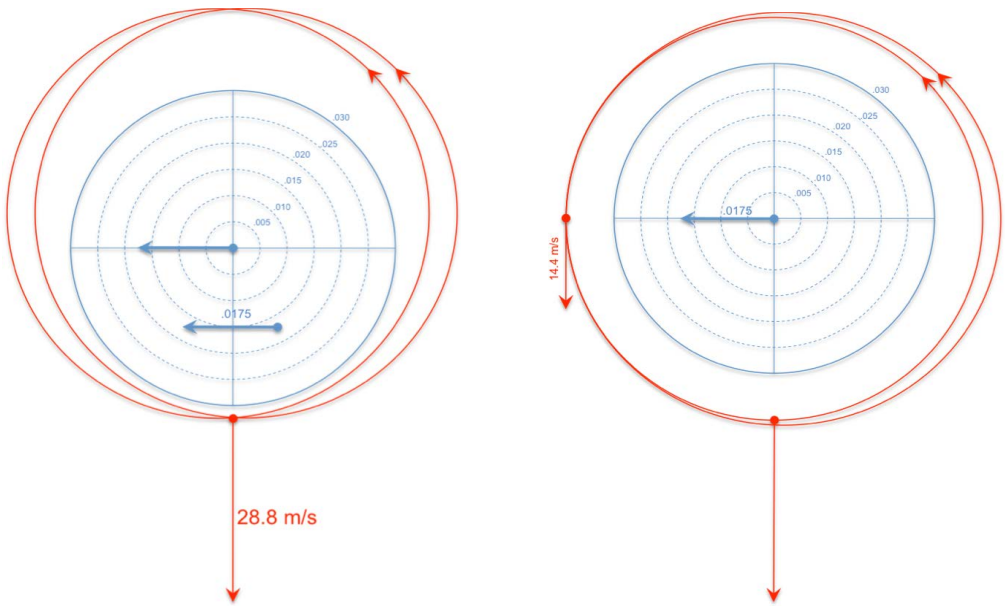

a) **b)**

Figure 2. Each of the figures above is a hybrid which shows polar coordinates for the central region of eccentricity space and then also identifies that with the central body in the orbit plane, so that orbits and maneuvers around the central body can be shown on the same plot. Part a) shows how changes in the eccentricity vector from a single radial impulse are the same for rotating the periapse and for moving away from circular (to see the latter, imagine that the orbits are moved down so they share a horizontal line of apsides with a circular orbit half way between them). Part b) shows how a half-sized tangential impulse has the same effect on the eccentricity vector as a radial maneuver in the same direction, though the orbit itself is also increased in size.

$$\|\Delta\mathbf{e}\| = 2e\sin\left(\frac{\Delta\omega}{2}\right) \approx \frac{\|\Delta\mathbf{v}\|}{v} \tag{6}$$

Now consider the case when we are doing a 180 deg transfer, i.e., reversing the periapse and apoapse. The maneuver would occur at the semi-latus rectum, which to first order in e is at a radius equal to a. So to first order, half the radial maneuver would take a circular orbit to one with eccentricity e, where (again ignoring terms in e^2):

$$\|\Delta\mathbf{e}\| = e \approx \frac{\|\Delta\mathbf{v}\|}{v} \tag{7}$$

which is also shown in Figure 2.

B. Easy Moves in Eccentricity Space II: Transverse Maneuvers

Now suppose we start at the center of eccentricity space, i.e., in a circular orbit. A transverse maneuver in the velocity direction puts us at periapse of a larger orbit, or in the anti-velocity direction puts us at apoapse of a smaller orbit. In the former case we can derive

$$v_p' = v_c\sqrt{(1+e)}$$

where v_p' is the periapse velocity in the new orbit, v_c is the velocity in the original circular orbit, and e is the eccentricity of the new orbit. Then again ignoring terms in e^2 we get

$$e \approx 2\frac{|\Delta v|}{v} = 2\frac{\|\Delta \mathbf{v}\|}{v} \tag{8}$$

where the latter equality follows from the tangency of the maneuver. Again the motion in the eccentricity space is at right angles to the direction of the maneuver. The same result can be derived when we have a maneuver in the anti-velocity direction.

C. A Geometric Interpretation

We've seen above that starting with a circular orbit, impulsive radial and tangential maneuvers give eccentricity vector changes that to first order in e have the same form as infinitesimal maneuvers. In the infinitesimal realm linearity holds, and we can break any perturbing acceleration up into radial and tangential components and then combine the effects of those components to get the effect of the original perturbing acceleration. But when we move to impulsive maneuvers of finite magnitude the situation is more complicated—we can again break the maneuver up into radial and tangential components, but as soon as one of those is applied we are no longer on a circular orbit. So in order to proceed, we need to know how maneuvers on elliptical orbits affect the eccentricity vector. We approach this geometrically, and the first step is to see geometrically what radial and tangential impulses do to a circular orbit.

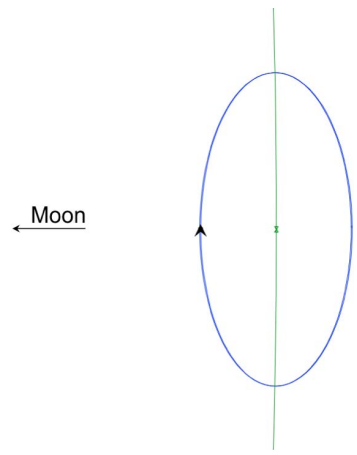

Figure 3. The basic Hill-Clohessy-Wiltshire representation of an elliptical orbit as an HCW ellipse around a reference point on a circular orbit in a rotating frame.

The Hills-Clohessy-Wiltshire equations linearize the dynamics in a rotating frame around a point in a circular orbit to find solutions which approximate nearby orbits; usually the rotating frame is aligned to have the central body on the $-x$ axis. These equations show (Fig. 3) that for any elliptical orbit that isn't too eccentric the motion relative to a point in circular orbit with the same period is an ellipse centered on and aligned along a vertical line through the point, with a semi-major axis of $2ea$ and a semi-minor axis of ea. Motion around the ellipse is simple uniform rotation at a rate of $-n$ around a small circle which is then stretched out along the semi-major axis direction, where n is the mean motion of both the original ellipse and the reference circular orbit.

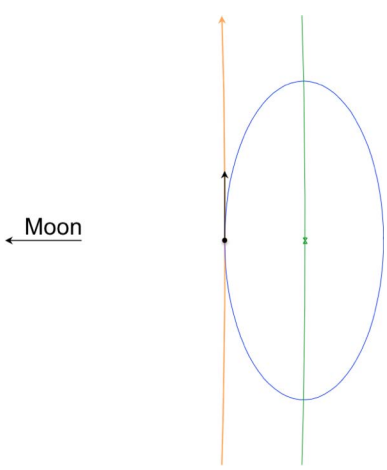

Figure 4. A tangential maneuver changes a circular orbit into an elliptical orbit representable as an HCW ellipse around a reference point on a larger circular orbit.

Now we can see visually what happens when we do a simple maneuver. A tangential impulse $\Delta\mathbf{v}$ changes the period of the orbit so that the orbiter is now on the inner edge of an HCW ellipse centered ea farther from the central body (Fig. 4), where to first order e is calculated according to Eq. (8). Similarly, an anti-velocity impulse puts the orbiter on the outer edge of an HCW ellipse centered ea toward the central body. A radial impulse Δv puts the orbiter on the tip of an HCW ellipse centered $2ea$ below or above the maneuver point for outward or inward impulses respectively (Fig. 5), where to first order e is calculated according to Eq. (7). Note that in both cases the distance the HCW center moves is approximately $2a\|\Delta\mathbf{v}\|/v$.

D. An Alternative Model which extends the HCW results

The basic HCW theory is incomplete in two ways: firstly, it only applies to orbits near a circular reference orbit; secondly, the solutions for a fixed reference point include HCW ellipses which are centered along the y-axis, instead of along the circular reference orbit (this is glossed over in Fig. 5). A geometric approach allows us an alternative extension of the HCW model which preserves the HCW ellipse around the origin of the rotating system, but which allows the origin to be on an elliptical reference orbit and places offset HCW ellipses along the reference orbit.

We begin by taking a different look at the basic HCW solution. When we transform the coordinate system from a rotating to a non-rotating frame[6], we find the model illustrated in Fig. 6. This shows an orbiter at periapse and shows that the motion of the orbiter is around a small circle at a rate of $2n$, an epicycle of radius $ae/2$, which is offset by a constant vector of length $3ae/2$ from the reference point which is the origin of the rotating coordinate frame. Rather than showing the central body moving around the reference point, we show the reference point moving on its circular orbit.

This is not a new model for two-body orbits—it was used by Copernicus. It is not hard to see that the orbit shape which it traces out is broader at right angles to the line of apsides than the distance from periapse to apoapse. Thus it is actually less accurate than the much older model of Ptolemy, which uses an eccentric circle called the deferent or excentric for the orbit shape and an equant to find position in the orbit. The equant is a point symmetrically opposite to the central body relative to the orbit center, i.e., it is the empty focus of the Keplerian ellipse which is the true two-body orbit in Newtonian dynamics. In Plolemy's model a point on the deferent moves uniformly around the equant at rate n; Copernicus showed that the point modeled using an epicycle as above also moves uniformly around the equant at rate n (as reported with great clarity in Ref. 7), and, as we see below, this motion matches very closely to that determined by Keplerian motion.

All of these models are accurate to first order in e, i.e., the error terms relative to a Keplerian ellipse involve squared or higher order powers of e. This information is implicitly contained in Cayley's tables[8], but is perhaps easier to see when the first order epicycle theory above is extended to higher order (in e) epicycle theory[2]. If we let $E(a,e,\omega,M_0)$ denote an orbit with the given semi-major axis, eccentricity, longitude of periapse, and initial mean anomaly and let $C(r,\dot{\alpha},\varphi)$ denote circular motion with the given radius, angular rate, and initial phase angle, so that

$$C(r,\dot{\alpha},\varphi)(t) = \begin{pmatrix} r\cos(\dot{\alpha}t+\varphi) \\ r\sin(\dot{\alpha}t+\varphi) \end{pmatrix}$$

then to third order in e (denoting the mean motion by n):

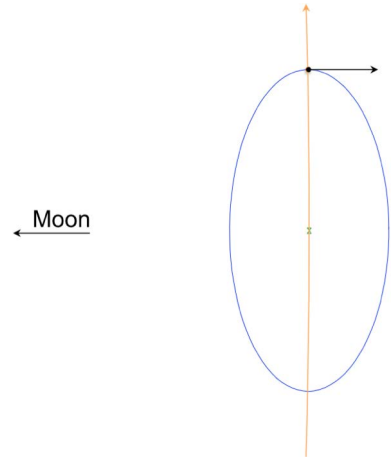

Figure 5. A radial maneuver changes a circular orbit into an elliptical orbit which has an HCW ellipse centered around a reference point which is offset along-track.

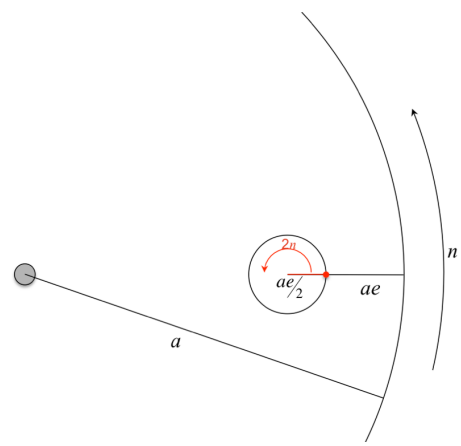

Figure 6. The first-order epicycle model for two-body motion. The reference point is on a circular orbit of radius *a*. There is a constant offset vector of length 3*ae*/2 in the opposite direction as the eccentricity vector and a small epicycle of radius *ae*/2 describing the path of a rotating radius vector which is aligned with the eccentricity vector at periapse and which rotates at a rate of 2*n* (as shown in red).

$$
\begin{aligned}
E(a,e,\omega,M_0) = {} & C(a,n,M_0+\omega) + C(\tfrac{3}{2}ae,0,\pi+\omega) + C(\tfrac{1}{2}ae,2n,2M_0+\omega) \\
& + C(\tfrac{3}{8}ae^2,3n,3M_0+\omega) + C(\tfrac{1}{2}ae^2,n,M_0+\pi+\omega) + C(\tfrac{1}{8}ae^2,-n,-M_0+\omega) \\
& + C(\tfrac{1}{3}ae^3,4n,4M_0+\omega) + C(\tfrac{9}{24}ae^3,2n,2M_0+\pi+\omega) \\
& + C(\tfrac{1}{24}ae^3,-2n,-2M_0+\omega) + o(e^4)\,.
\end{aligned}
\tag{9}
$$

But what if we want to start with an elliptical reference orbit—how do we transform Eq. (9) when the first term on the right is a reference ellipse instead of the reference circular orbit? Algebraic manipulation of Eq. (9) can show this directly, but in keeping with our geometric theme that derivation is left as an exercise for the interested reader (or the student of one). The geometric answer is illustrated in Fig. 7. We start with two orbits modeled with epicycles and consider first just the first-order part of the model. Because we are concerned with the relative shapes of the orbits, we are free to move to a common reference point at the ascending node; at this point the mean anomaly, M_0, is $-\omega$ for each orbit so that the initial phase angle on the reference orbit is 0 and the initial phase angle in the first-order epicycle is also $-\omega$, which makes the initial epicycle vector equal to one-third of the negative of the vertical reflection of the offset vector. This relationship between the offset and the epicycle vector at the ascending node is a defining characteristic of the first-order epicycle model.

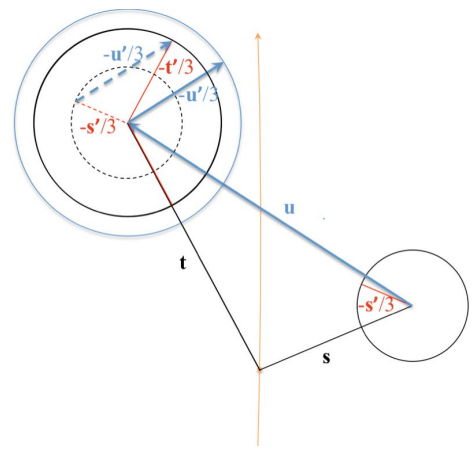

Figure 7. Illustrating a demonstration that motion in an ellipse relative to another elliptic orbit can be modeled to first order using the same offset and epicycle model as applies with respect to a circular reference orbit.

To model one ellipse relative to the other, we subtract the second model from the first. Since we are doing vector arithmetic we are free to reorder the subtraction so that we subtract the offset vectors and then add the difference of the epicycles. The difference of the offset vectors, **t-s**, is labeled **u**, and we also derive immediately that (-**t′**/3 – (-**s′**/3)) = -**u′**/3, thus the difference of the offset vectors at the ascending node is exactly what characterizes the epicycle model. Furthermore, since the rate of rotation for both epicycle vectors is $2n$, their difference rotates at the same rate.

Thus the epicycle model for one ellipse relative to another is exactly the same to first order as the model relative to a circular reference orbit. Terms which are second-order and higher in e remain so. One further difference to note is that when the reference orbit is a circle is is easiest to think of the offset vector as being –(3/2)**e**, but now we need to identify it with –(3/2)Δ**e**; this is not actually a change in the modeling paradigm, since for the circular reference orbit, i.e., for the ellipse with respect to a circular orbit, we have **e**=Δ**e**.

Now for the twist that was mentioned in the introduction. Since we have a first-order model for motion relative to a point in an elliptical orbit in an inertial frame, we can convert to a rotating frame centered on the reference point and rotating at the rate n. Just as before but in the opposite direction of conversion we get the HCW ellipse shown in Fig. 3 centered on the reference point. The twist is that the orientation of the rotating frame—in which the HCW ellipse is fixed—is determined by the mean anomaly of the reference point, while the position of the reference point on the ellipse is determined by the true anomaly. In this rotating frame the central body is not fixed on the negative x-axis but oscillates above and below it as the true anomaly gets ahead of and behind the mean anomaly. So we can break a maneuver up into components just as before, and analyze their effects as shown in Figs. 4 and 5, but the definitions of transverse and radial are with respect to the mean anomaly instead of to the true anomaly, i.e., we have to separate the maneuver into components in a frame twisted by the difference between mean and true anomaly. When that is done we get the result given in Eq. (1).

III. Application to Maneuver Design

The basic geometry relating maneuvers to changes in the eccentricity vector allows us to answer some mission design questions immediately. For example, suppose we want a low polar lunar orbiter in orbit for a year and keep it nadir oriented; since the gravity field will push the eccentricity vector to the right as shown in Fig. 1 we will need

to do orbit maintenance maneuvers to move the eccentricity vector back to the left and we want to do them over one of the poles where we have multiple coverage of the surface. How should we mount our thruster for orbit maintenance? We can immediately suggest that it be mounted on top of the spacecraft to do a radial thrust down over the north pole and at the same time observe that we only get half the observing time from the same propellant load as if we did tangential maneuvers over the equator so that a trade between observing time and interruptions at the equator can be considered.

To extend this example, suppose we decide to accept the equatorial interruptions to optimize propellant usage by using tangential maneuvers, but we want to keep the period constant for ground track control. Then we immediately know that a single maneuver can't do the job. But if we use a pair of maneuvers on opposite sides of the equator, we can do one in the velocity direction and one in the anti-velocity direction so that the eccentricity vector changes add up (since the two maneuvers are in the same direction inertially) but the period changes cancel, a strategy reminiscent of Hohmann transfers.

In the following sections, we consider more detailed use of the geometric model defined by Eq. (1).

A. Incorporating Desired Period Changes

Since we decompose every maneuver into components which are at right angles, and their effects in eccentricity vector space are at right angles to the maneuver components, the effects are themselves at right angles to each other. That means that every maneuver to perform a given eccentricity change can be decomposed into a right triangle in eccentricity vector space whose hypotenuse is the eccentricity change and whose legs are the changes resulting from the transverse and radial components of the maneuver. The vertices of all possible maneuvers to do a given eccentricity vector change thus form a circle with the given eccentricity vector change as the diameter, as shown in blue in Fig. 8.

If there is a specific period change to incorporate into the maneuver, then that determines the length of the transverse component of the maneuver (3.3 m/s on the left side of Fig. 8). This means that if we order the components with the transverse maneuver first, exactly two points on the circle represent the combination of transverse and radial components that give the desired period change and eccentricity vector change, one of which is shown in Fig. 8 and the other being a reflection across the desired $\Delta\mathbf{e}$.

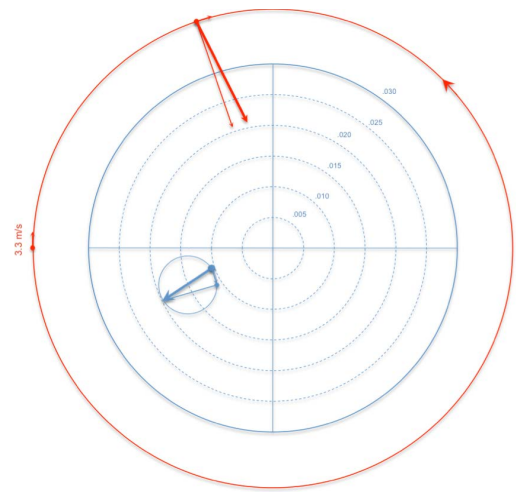

Figure 8. An example of a maneuver that is one of only two that can achieve this specified $\Delta\mathbf{e}$ and period change simultaneously.

Once we have in hand a particular $\Delta\mathbf{e}$ from the transverse component of a maneuver we know the direction of the transverse component, and that in turn fixes the position in orbit where the maneuver must be executed. The radial component is similarly defined and equally determines the maneuver position. Note that although the components and their effects all relate by right angles, the total $\Delta\mathbf{e}$ is not exactly at right angles from the total maneuver because the effects of the two maneuver components scale differently from the maneuver components; this was discussed above at the end of the introductory part of section II.

One final twist is that because the starting $\mathbf{e}$ is non-zero we need to turn the maneuver components and move the reference point by the difference between mean and true anomalies at the maneuver point, which difference in this case is near maximum because the reference point is about at right angles to the line of apsides. But since the reference ellipse eccentricity is only 0.01, the twist is just over a degree (arcsin(0.02)), which is negligible in this context. And the effect on the period change from the twist is even smaller, of order e^2.

B. Incorporating Orbit Plane Changes

As we've just seen, specifying the $\Delta\mathbf{e}$ and period change pretty much determines what maneuver is needed, so there is no freedom in choosing the maneuver location to effect a desired plane change with the same maneuver. All the same we would like to preserve the Δv savings that come from combining maneuver components into a single maneuver. The geometric approach allows us to see how requirements for eccentricity vector change and plane change interact in the presence of a specific period change. Then multiple maneuvers can be combined to make all the desired changes most efficiently.

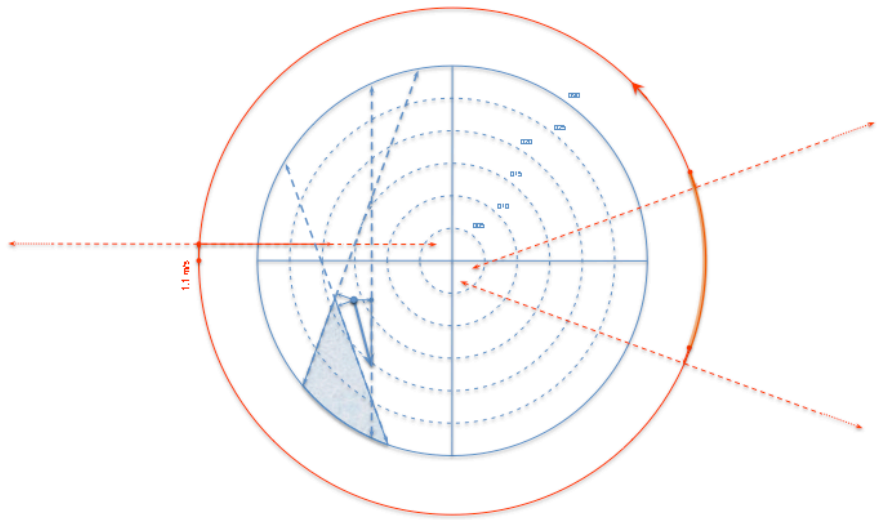

Figure 9. Given a particular period change and a need to do the maneuver within 20 deg of the x-y plane (so that inclination change is efficient), only the shaded region of the eccentricity space is accessible.

Figure 9 shows how what's possible in changes to the eccentricity vector can depend on constraints on how much the period should change and what plane change is desired. The size and direction of the red tangential maneuver on the left in the figure is determined by a desired period change, and its position is constrained to one of two positions by the desire to cause a pure inclination change. The red horizontal dashed line at the tip of it shows all possible radial maneuver components that can combine with it and keep the period and plane changes fixed; one example radial component is selected as a solid arrow. The effect in eccentricity space is shown in blue—the example maneuver gives us a $\Delta\mathbf{e}$ which is down and to the right and we can achieve just the eccentricity vector positions on the blue dashed vertical line by changing the size of the radial maneuver component.

Choosing the other node of the orbit would allow an alternative vertical line of possible positions to be reached in eccentricity space equally far to the left of the original position instead of to the right. By accepting a little inefficiency in the plane change we can open up the area available in eccentricity space. The range of maneuver positions on the right is within 20 deg of the ascending node so the worst inefficiency in getting a desired inclination change in the out-of-plane component is less than 6.5%, and the inefficiency in the total maneuver is less. Moving away from the node also introduces change in the longitude of the ascending node into the plane change, but this can be reversed in a subsequent maneuver, which may or may not share the burden of inclination change.

I have framed this discussion in the context of inclination and node change to make it easier to describe the changes, but it applies equally well to any desired plane change. Note in passing that no radial maneuver can cancel out the change from the tangential component, i.e., it is impossible to change the period in a single maneuver without changing the eccentricity vector of an orbit.

C. GRAIL's Transition to Science Formation (TSF)

The GRAIL mission begins its TSF Phase with the GRAIL-B orbit larger than the GRAIL-A orbit, and both outside the science orbit. A series of TSF maneuvers (TSMs) will systematically step down the periods of the orbits at times designed to establish and progressively refine the phase relationship between the orbiters. The period reductions for GRAIL-A are 14.4 s and 29 s, with tangential Δv components of 1.4 m/s and 2.3 m/s respectively; the period reductions for GRAIL-B are 180 s, 25 s, and 4 s, with tangential Δv components of 14.4 m/s, 2.0 m/s, and 0.4 m/s respectively. At the same time, radial and out-of-plane maneuver components will adjust the eccentricity vector so that the science phase starts with GRAIL-B's eccentricity vector on the left and close to GRAIL-A's eccentricity vector and will adjust GRAIL-B's orbit plane to match GRAIL-A's orbit plane. In order to analyze the effects of maneuver execution errors on the size and timing of subsequent maneuvers through the TSF Phase, GRAIL mission designers have constrained the total sizes of the TSMs to 21 m/s for GRAIL-A and to 30 m/s, 7 m/s, and 2 m/s for GRAIL-B.

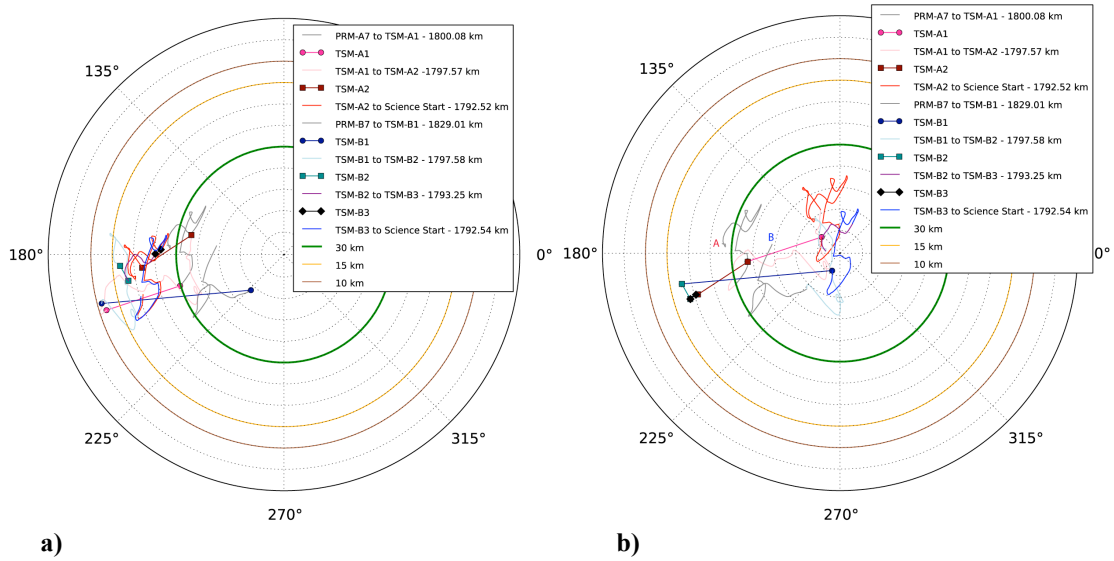

Figure 10. Orbit evolution and maneuvers in the GRAIL Transition to Science Formation Phase. Figure 10a shows the effects of the orbit evolution segments and the TSMs in the order they happen, while Fig. 10b reorders them to move all the maneuvers to the end of the TSF, making the cumulative maneuver effects clearer for each orbiter. (Figure provided by Sara Hatch at JPL.)

The evolution of the orbits and changes from maneuvers in eccentricity space are shown in Fig. 10a. Since the evolution of the eccentricity vector caused by the gravity field of the Moon is quite independent of where it is in the eccentricity plot, and the maneuver effects are similarly independent of initial location, I have reordered the segments of the orbit evolution and the maneuver effects to gather all the maneuver effects at the end as shown in Fig. 10b. This points out that the end points of the TSF Phase are very close together for the two orbiters and lets us see the total eccentricity change desired from maneuvers. We can see directly from Fig. 10b that the combined maneuvers for each orbiter need to result in a $\Delta\mathbf{e}$ which is to the left and about 0.20 in magnitude (to convert to the units of Fig. 10, a Δe of 0.20 is about 35 km change in periapse altitude).

Given the constraints on the TSMs which are described above, each maneuver can achieve the region of possible $\Delta\mathbf{e}$ which by is shown in Fig. 11 (since TSM-B3 is so small on this scale, it is left out). Each region is an annulus, where the inner region is "forbidden" because the prescribed period changes determines a tangential maneuver component which in turn entails a minimum $\Delta\mathbf{e}$ which can only be increased by a radial maneuver component. The outer boundary of the annulus is actually somewhat flexible because it is determined by the amount of Δv allocated to the radial maneuver component. To generate the figure, I decomposed the total maneuver allocation into the prescribed tangential component and a cross-track component, which I then allocated equally into radial and out-of-plane components. If a particular maneuver does not require any out-of-plane component then more can be used in the radial component; in TSM-B1, for example, the length of the vertical line showing possible radial maneuver effects would increase by 41%, which gives an 85% increase in the width, or thickness, of the annulus. The "forbidden" regions for the GRAIL-A TSMs are much smaller, so the gain from reallocating Δv from out-of-plane to radial basically increases the diameter of the annulus by about 40%.

We can see immediately from Fig. 11 that the GRAIL-A TSM maneuvers will need to be positioned near the equator with large radial components relative to the tangential component. This means that inclination changes will be efficient but that node changes will be difficult. Fortunately, this dovetails well with the mission requirements, which do not include any constraint on the longitude of the ascending node of GRAIL-A. It is similarly clear that most of the $\Delta\mathbf{e}$ needed for GRAIL-B will be accomplished by TSM-B1 and it will need to be positioned roughly near the ascending node. There is much more freedom in placement of TSM-B2 since the period-change contribution to the $\Delta\mathbf{e}$ is relatively small and TSM-B1 can be adjusted to compensate for direction swings in TSM-B2; this is consistent with the rule of thumb developed by Sara Hatch in her TSF maneuver design work that plane changes to match the GRAIL-B orbit plane to GRAIL-A's should be done at TSM-B2.

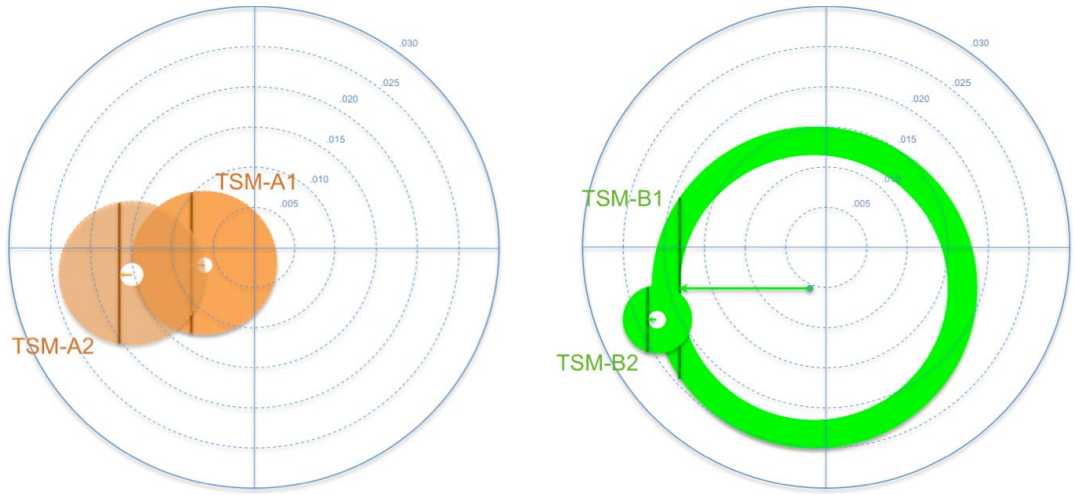

a) **b)**

Figure 11. The possible endpoints for the first two TSMs for GRAIL-A (on the left) and GRAIL-B (on the right), relative to a typical starting point in eccentricity space. The inner edge for each annulus is determined by the period change of that TSM, whose effect is shown by an arrow, and the outer edge is given by the allocation for the radial component of the maneuver, whose effect is shown by a vertical line indicating the possible endpoints depending on the size of the radial maneuver component. As the maneuver position in orbit is varied, the effects of the maneuver components rotate around the initial eccentricity position, sweeping out the shaded annulus.

IV. Conclusion

All of the initial maneuver design for GRAIL has been done before the geometric analysis which is described here was developed. Optimization code was used to determine maneuver parameters while meeting certain constraints on period, etc., with a lot of challenging and time-demanding user interaction[2]. The geometric insight described in this paper can be used to find initial guesses for maneuvers that can then be optimized with the inclusion of higher order terms and with the maneuvers modeled as finite burns instead of as impulses. This geometric method can also be used to validate (or invalidate) a maneuver strategy for achieving desired orbit changes. Such application in the GRAIL mission design is under way and should prove most valuable in operations, when the maneuver design process is very time-constrained during the TSF Phase.

Besides providing a first-order theory which can be applied geometrically, the development given above can be extended to second-order explicitly using Eq. (9). There is room also for more detailed explication of the maneuver twist applied when the initial eccentricity is non-zero.

Acknowledgments

I thank Tim McElrath at JPL for telling me about the relationship between perturbing acceleration and motion in eccentricity vector space, and he in turn thanks Tomas Martin-Mur at JPL for introducing it to him. I also thank Prof. John Cochran of Auburn University for telling me about Cayley's tables. And I thank Sara Hatch at JPL for the plots in Figs. 1 and 10. This research was performed at the Jet Propulsion Laboratory, California Institute of Technology, under contract with the National Aeronautics and Space Administration.

References

[1] Roncoli, R. B., Fujii, K. K., "Mission Design Overview for the Gravity Recovery and Interior Laboratory (GRAIL) Mission," *AIAA/AAS Astrodynamics Specialist Conference*, 2010 AIAA Meeting Papers on Disc, Vol. 15, No. 9 (GNC/AFM/MST/Astro/ASE), AIAA, Washington, DC, 2010 (submitted for publication).

[2] Hatch, S. J., Roncoli, R. B., and Sweetser, T. H., "GRAIL Trajectory Design: Lunar Orbit Insertion through Science," *AIAA/AAS Astrodynamics Specialist Conference*, 2010 AIAA Meeting Papers on Disc, Vol. 15, No. 9 (GNC/AFM/MST/Astro/ASE), AIAA, Washington, DC, 2010 (submitted for publication).

[3] Battin, R. H., *An Introduction to the Mathematics and Methods of Astrodynamics*, AIAA Education Series, AIAA, New York, 1987, p. 499.

[4] Carrou, J.-P. (ed.), *Spaceflight Dynamics, Part I*, Cepadues-Editions, Toulouse, France, 1995, p. 350.

[5] Phong, C., and Sweetser, T. H., "Minimum Impulse Transfers to Rotate the Line of Apsides," *Astrodynamics 2005*, edited by Kathleen C. Howell, Bobby Williams, Felix Hoots, and Louis D'Amario, Advances in the Astronautical Sciences, Vol. 123, Univelt, San Diego, CA, 2006, pp. 1901-1910.

[6] Sweetser, T. H., "Epicycles and Oscillations: the Dynamics of the LISA Orbits," *Astrodynamics 2005*, edited by Kathleen C. Howell, Bobby Williams, Felix Hoots, and Louis D'Amario, Advances in the Astronautical Sciences, Vol. 123, Univelt, San Diego, CA, 2006, pp. 693-712.

[7] Gingerich, O., *The Book Nobody Read*, Walker & Co., New York, 2004, pp. 263-265.

[8] Cayley, A., "Tables of the Developments of Functions in the Theory of Elliptic Motion," *Mem. Roy. Astron. Soc., 29* (1861), pp.191-306.